Targeting of Single-Stranded Oligonucleotides through Metal-Induced Cyclization of Short Complementary Strands

by **Fabrice Freville**[a])[b]), **Tristan Richard**[a])[b]), **Katell Bathany**[c]), and **Serge Moreau***[a])[b])

[a]) INSERM U386, Bordeaux, Université Victor Segalen Bordeaux 2, 146 rue Léo Saignat, F-33076 Bordeaux Cedex (e-mail: serge.moreau@bordeaux.inserm.fr)

[b]) Université Victor Segalen Bordeaux 2, 146 rue Léo Saignat, F-33076 Bordeaux Cadex

[c]) Institut Européen de Chimie et de Biologie (IECB), 2 rue Robert Escarpit, F-33607 Pessac Cedex

A new strategy to cyclize short synthetic oligonucleotides on DNA or RNA target strands is described. The approach is based on metal-templated cyclization of short synthetic oligonucleotides conjugated with two chelating 2,2′:6′,2″-terpyridine (Tpy) moieties at their 3′- and 5′-ends. Cyclization after metal addition (Zn^{2+}, Fe^{2+}) was demonstrated by means of thermal-denaturation experiments, MALDI-Q-TOF-MS, and gel electrophoresis (PAGE). 1D- and 2D-NMR Experiments were performed to analyze the association of complementary strands after metal-mediated cyclization. Our protocol allows the efficient circularization of synthetic oligonucleotides. Thereby, the hybridization on a complementary strand was more efficient with an RNA target strand and a 2′-*O*-methylated circularized oligomer.

1. Introduction. – RNA can form stable structures with a small number of nucleotides. Combination of various secondary structural elements can lead to tertiary structures of increasing complexity [1]. Such structures are involved in numerous regulation processes through interactions with RNA, DNA, or proteins [2]. The iron-responsive element (IRE), a hairpin structure present in mRNAs coding for key proteins in the iron metabolism of vertebrate cells, is a good example [3]. Numerous examples of functional RNAs are also found in viruses, an example being TAR RNA, the RNA sequence required for transactivation of the transcription of the HIV-1 genome [4]. Ligands designed to target such RNA motifs may allow the control of the metabolic processes that they mediate.

We are interested in strategies aiming at locking, through catenane formation, synthetic oligonucleotides on hairpin motifs of RNA, an essential secondary structure of RNA often involved in regulation of gene expression [3]. Catenanes are intertwined polymembered rings tied together [5][6]. Such bulky synthetic complexes on RNA hairpin may allow an efficient inhibition of the association of the natural ligands of these structures. Our first attempt in this line is developed here, based on modified oligonucleotides bearing terminal 2,2′:6′,2″-terpyridine (Tpy) moieties for the addition of metal ions and formation of a catenane structure with the targeted hairpin motif (*Fig. 1*,*a*).

Cyclic [7], polymeric [8], and chiral assemblies [9] could be obtained by means of the chemistry of terpyridines and their metal complexes. Physiologically available ions such as Zn^{2+} could be recruited to mediate such a process [10]. The high dynamic characteristics of Zn–$(Tpy)_2$ complexes should allow an easy closing of the ligand on a

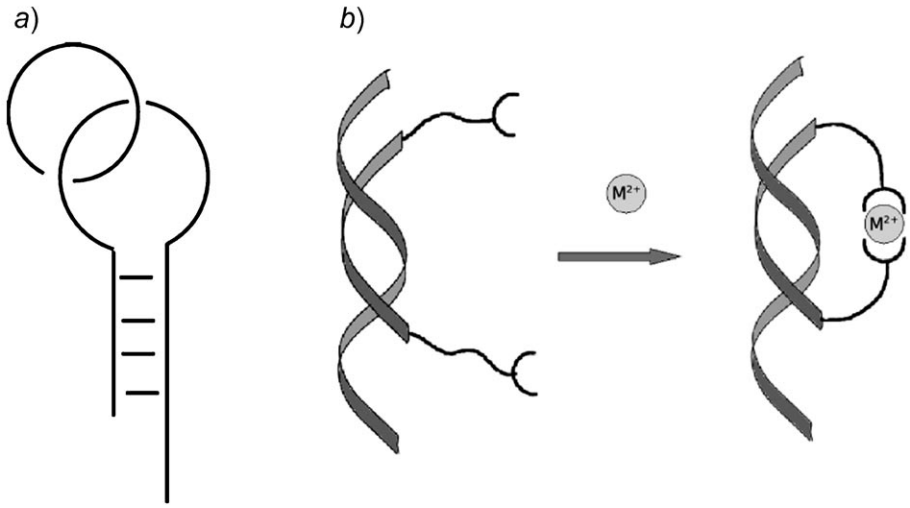

Fig. 1. a) *Schematic representation of a circularized oligonucleotide with a catenane.* b) *Metal-templated cyclization of a bis-terpyridine-modified oligonucleotide on a target strand.*

RNA hairpin [11]. We previously developed methods of conjugation of terminal Tpys on synthetic oligomers and showed that metallic coordination leads to a large increase in the stability of duplexes or short hairpins [12]. In order to evaluate the ability of Tpy-modified oligonucleotides to cyclize around the targeted strand, we designed a simplified system where the DNA or RNA target strand is a short linear sequence allowing the formation of a 9-bp (bp = base pair) duplex with the Tpy-modified oligomer. Such a one-turn helical duplex will put the 3′- and 5′-Tpy residues in a face-to-face conformation allowing easy closing through metal coordination and leading to a target strand passing through the circularized Tpy oligomer (*Fig. 1*, *b*). This topology is a prerequisite for the formation of the interlocked rings of a catenane structure.

The target oligomer sequences were derived from a RNA hairpin of the internal ribosomal entry site (IRES) of the hepatitis-C virus (HCV). The apical loop of the domain IIIb of this IRES fulfils some of the above-mentioned criteria. First, it is involved in the IRES function by recruiting essential co-factors of translation initiation such as eIF3 [13]. Second, the length of the loop (14 nt) allows the hybridization of a complementary strand leading to one-turn helical double helices.

2. Results. – 2.1. *Oligomer Sequences.* All strand sequences are shown in *Table 1*, together with selected mass-spectrometric data. Either DNA or RNA sequences were used as targets. The complementary strands were DNA and 2′-*O*-methylated oligonucleotides.

2.2. *Molecular Modeling and Chemical Synthesis.* We chose a new chemical approach [14] for the synthesis of bis-terpyridine (Tpy_2)-conjugated oligonucleotides. It relies on the use of (*R*)-2,4-dihydroxybutyramide *seco*-pseudonucleosides as substitute for nucleosides, as shown by *Dioubankova et al.* [15]. This synthon allows the introduction of various ligands or labels at both ends of oligonucleotides through phosphor-

Table 1. *Numbering and Sequences of Strands Used in this Study.* Abbreviations: **r** and **m** stand for ribonucleotide and 2′-*O*-methylated ribonucleotide, resp. The MS data were obtained on a MALDI-Q-TOF mass spectrometer (±0.01 Da). For details, see *Exper. Part.*

Strand	Sequence	$[M-H]^-$ [*m*/*z*]	Calc. isotopic mass [Da]
1	5′-GGTCCTTTCTTGG-3′		
1r	5′-GGUCCUUUCUUGG-3′		
2	5′-CCTTTCTTG-3′		
2r	5′-CCUUUCUUG-3′		
3	5′-CAAGAAAGG-3′		
3m	5′-CAAGAAAGG-3′		
4	5′-CAAAAAAGG-3′		
5	5′-CAAGAAAGGP-3′	3361.75	3362.76
5m	5′-CAAGAAAGGP-3′	3631.84	3632.85
6	5′-PCAAGAAAGG-3′	3361.75	3362.76
7	5′-PCAAGAAAGGP-3′	3944.95	3945.98
7m	5′-PCAAGAAAGGP-3′	4215.06	4216.07
8	5′-PCAAGAAAGGTP-3′	4249.00	4250.02
8m	5′-PCAAGAAAGGUP-3′	4535.09	4536.11
9	5′-PTCAAGAAAGGTP-3′	4553.04	4554.07
9m	5′-PTCAAGAAAGGTP-3′	4823.21	4824.16

amidite chemistry, and the synthesis of a specific solid support. To define the length of the chemical link between the Tpy moieties and the 3′- and 5′-OH groups of the cyclic oligomer (see *Fig. 1*), we built an initial duplex using an ideal *A*-form double-helical model. The coordination link and geometry of the Tpy units were constrained according to the X-ray coordinates of known Fe complexes [16]. The general structure of Tpy-conjugated oligomers and a representation of the optimized structure of the hybridized *A*-form duplex is shown in *Fig. 2*,*a* and *Fig. 2*,*b*, respectively.

2.3. *Melting-Temperature Experiments.* As a first analysis of the putative circularization of the Tpy-modified oligomer around its target, we designed various combinations of complementary strands and followed their association by UV-monitored thermal-denaturation experiments. Three kinds of duplexes were used: type-0 duplexes for non-conjugated oligomers, type-I duplexes for mono-terpyridine (Tpy) conjugates, and type-II duplexes for the bis-terpyridine (Tpy_2) ones. Strand associations were studied in both metal-free buffer (10 mM phosphate buffer (pH 7.0), 150 mM NaCl, 200 μM EDTA) and in the presence of control amounts of Zn^{2+}, Fe^{2+}, and Ni^{2+} in the same buffer, but without 'ethylenediamine tetraacetate' (EDTA). Added equivalents refer to the duplex concentration (1 μM). The experimental data for DNA targets are collected in *Table 2*.

Denaturation of the samples was carried out by increasing the temperature from 4 to 90°. The melting temperature (T_m) was derived through graphical methods, with an uncertainty of ±1°. A striking feature of these data are that type-II duplexes exhibited a significant drop in T_m values compared to any other strand associations. Although thermal data were difficult to determine in these cases, a melting transition ($T_m = 10–20°$) with a significant hyperchromic effect was observed on heating.

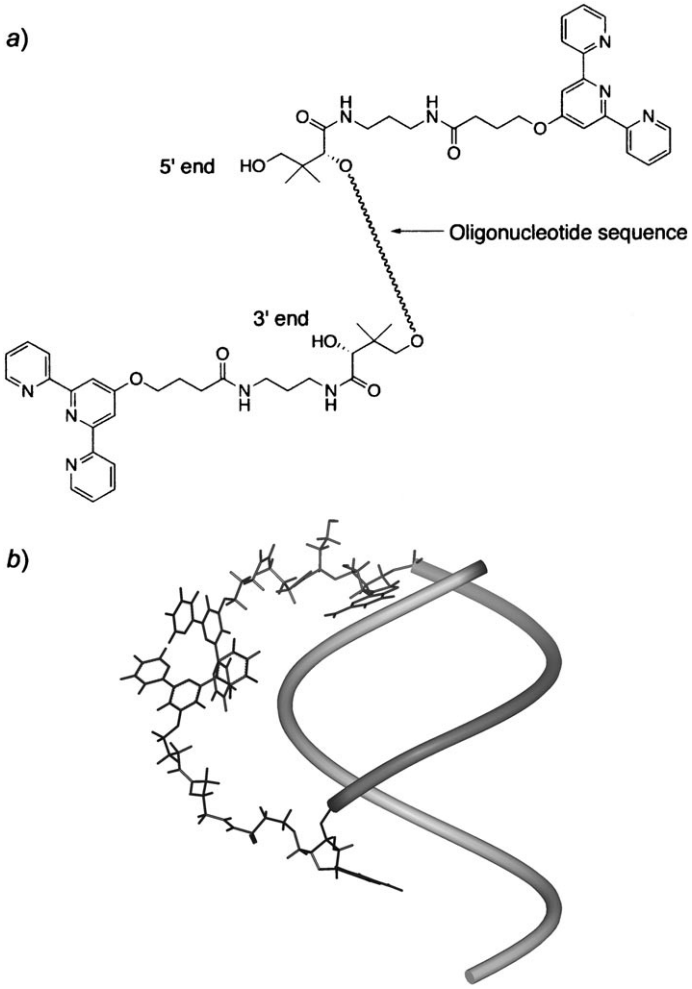

Fig. 2. *Chemical structure of bis-terpyridine-conjugated oligonucleotides* (*a*) *and optimized structure of the* A*-form duplex with constrained Tpy distances* (*b*)

In *Fig. 3*, the typical transitions of duplexes **0a** and **IIa** in the presence of 1 equiv. of Zn^{2+} are shown. Type-II duplexes were clearly formed at low temperature. For comparison, a mismatch duplex (**0b**, see *Table 2*) was thermally investigated, but failed to show a melting transition. Type-0 duplexes showed expected T_m values, both in metal-free buffer or with added metal ions, with slight variations around 29.0°. The melting temperatures of type-I duplexes (one strand with one Tpy moiety) were found to be rather insensitive to metal addition. A slight contribution of the Tpy to the stability of the duplexes was detected even in metal-free buffer. Such a behavior has been reported previously [12]. Thus, the specific behavior of type-II duplexes is related to the presence of the two Tpy moieties at the 3′- and 5′-ends of one strand. Extension of the link between the two conjugated Tpys by intercalation of one or two unpaired T

nucleobase(s) did not result in a different behavior, as can be seen by comparing the T_m data for **IIa**, **IIb**, and **IIc** in *Table 2*.

Table 2. *Melting Temperatures* (T_m) *or Melting-Temperature Ranges of DNA Duplexes Formed by Strand Association*. For definition of strands, see *Table 1*. All T_m values (±1°) are mean values of at least three experiments. Solvent: 10 mM aq. phosphate buffer (pH 7.0) containing 150 mM NaCl.

Duplex	Strands	T_m [°]						
		No metal[a])	Zn^{2+} (1)[b])	Fe^{2+} (1)	Ni^{2+} (1)	Zn^{2+} (20)	Fe^{2+} (100)	Ni^{2+} (2)
0a	**1/3**	28.9	28.3	29.5				
0b	**1/4**	n.t.[c])	n.t.					
Ia	**1/5**	31.2	31.6	32.3				
Ib	**1/6**	33.5	34.6	35.0				
IIa	**1/7**	35.1	10–20	10–20	10–20	28.3	10–20	42.4
IIb	**1/8**	35.0	10–20	10–20	10–20			
IIc	**1/9**	34.2	10–20	10–20	10–20			
0c	**2/3**	26.5	24.9	26.4				
Ic	**2/5**	29.1	30.4	29.0				
Id	**2/6**	33.4	33.6	32.9				
IId	**2/7**	34.0	10–20	10–20			10–20	36.4
IIe	**2/8**	32.8	10–20	10–20	10–20		10–20	36.6
IIf	**2/9**	32.6	10–20	10–20			10–20	36.1

[a]) With metal-free buffer, prepared as described in the header, but completed with 200 μM EDTA. [b]) In parentheses, the equivalents of metal relative to duplex concentration (1 μM) are given. [c]) No transition observed.

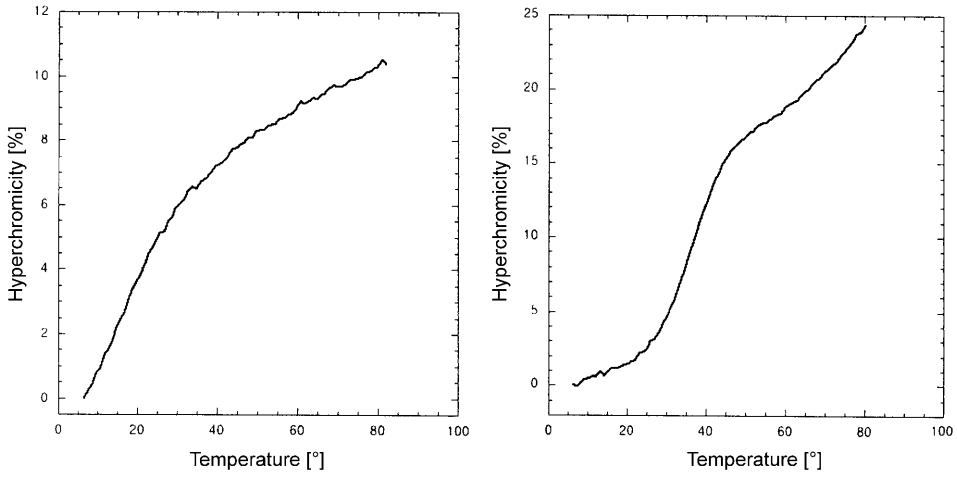

Fig. 3. *Thermal melting curves of duplexes* **0a** (right) *and* **IIa** (left) *in the presence of* Zn^{2+} (1 equiv.). Conditions: aq. phosphate buffer (pH 7), 150 mM NaCl, duplex/Zn^{2+} 1:1 (1 μM each), heating rate 0.5°/min, UV monitoring at 260 nm.

To take into account the potential effect of dangling nucleotides of the target strand **1**, when hybridized to its complementary oligomer, we studied various duplexes including a shorter target strand, allowing the formation of blunt-end duplexes (Strand **2**, *Table 1*). As revealed in *Table 2*, these new duplexes, *i.e.*, **0c**, **Ic**, **Id**, and **IId**–**f**, were found to exhibit a very similar behavior to that observed for duplexes **Ia**–**IIc**. Type-II duplexes always had T_m values in the range 10–20°. Thus, the dangling ends of the target cannot be responsible for these specific drops in melting temperature.

Metallation of the $(Tpy)_2$-type strands **7**, **8**, or **9** was associated with a drop in T_m. This suggested that the link between the two Tpy units through metal complexation is involved. We then added excess of metal ions to promote the formation of mono-metallated entities and thus disrupt the coordination link between the two nearby Tpy residues. In general, this can be easily achieved through addition of a slight excess of Ni^{2+} or larger amounts of Zn^{2+} [12][17]. As can be seen from *Table 2*, a ratio of 2:1 for Ni^{2+}/duplex or of 20:1 for Zn^{2+}/duplex led to a significant increase in melting temperature ($T_m = 28.3–42.4°$) of duplexes **IIa**–**f** relative to a 1:1 metal/duplex mixture ($T_m < 20°$). Further, as predicted from thermodynamics and kinetics data [11][17], even a large excess of Fe^{2+} failed to promote the formation of mono-metallated Tpy.

We extended our studies to RNA targets and 2′-*O*-methylated ligands. The experimental data are listed in *Table 3*. As expected for such strand combinations, we observed a raise in T_m values compared to those of the (similar) duplexes of *Table 2*. For example, the unmodified duplex **0r** exhibited a melting temperature of 40.4°, which is 11.5° higher than that of the corresponding duplex **0a**. Type-II duplexes exhibited cooperative melting transitions, allowing the determination of T_m in this case. However, upon addition of 1 equiv. of metal ion, we always noticed a drop in T_m of these duplexes ($T_m \approx 10°$) compared to those of type 0 and type I (*Table 3*). A slight excess of Ni^{2+} (2:1 metal/duplex) also led to an increase in T_m, revealing the disruption of the coordination link between the two Tpy moieties. A noticeable difference between DNA and RNA strands was that extension of the link between the Tpy units resulted, in this special case, in an increase in T_m. Insertion of one or two unpaired T nucleobases in the target strand (duplexes **IIrb** and **IIrc**) increased T_m from 29.9 to 37.3° (*Table 3*).

Table 3. *Melting Temperatures* (T_m) *of Studied RNA Duplexes.* All T_m values (±1°) are mean values of at least three experiments. Solvent: 10 mM aq. phosphate buffer (pH 7.0) containing 150 mM NaCl.

Duplex	Strands	T_m [°]						
		No metal[a])	Zn^{2+} (1)[b])	Fe^{2+} (1)	Ni^{2+} (1)	Ni^{2+} (2)	Zn^{2+} (1) + Mg^{2+} (3 mM)	Zn^{2+} (1) + Mg^{2+} (10 mM)
0ra	**1r/3m**	40.4	40.3	40.6			40.0	41.8
Ira	**1r/5m**	41.4	42.2	41.7				
IIra	**1r/7m**	43.3	29.9	29.4	31.4	39.8	33.5	42.8
IIrb	**1r/8m**	44.6	33.2	36.2	35.0	43.1	39.0	44.3
IIrc	**1r/9m**	43.3	37.3	37.1	35.7	41.2	42.4	46.6

[a]) In metal-free buffer, prepared as described in the header, but completed with 200 μM EDTA. [b]) In parentheses, the equivalents of metal relative to duplex concentration (1 μM) are given.

An interesting observation was made when Mg^{2+} was added to the **IIr** duplexes. In these cases, the T_m values observed for $(Tpy)_2$-modified oligomers reached or, in some cases, even exceeded those determined for the unmodified duplex **0r** (*Table 3*). Thus, the duplex **IIrc** composed of the RNA strand **1r** and the extended 2′-*O*-methylated ligand (**9m**; see *Table 1*), were melting at 46.6°, *i.e.*, 4.8° above T_m of the unmodified duplex **Ir** (T_m 41.8°) under the same experimental conditions. At physiologically relevant Mg^{2+} concentration (3 mM), the increase in T_m was 2.4°.

2.4. *Mass-Spectrometric Analysis.* The stoichiometry of various metal complexes was studied by mass spectrometry (MS). Prior to MS measurements, single- or double-stranded oligomers were metallated under the same experimental conditions (concentration, buffer, pH) as reported above for thermal-denaturation experiments. An aliquot was then sampled, and the buffer was exchanged for ammonium acetate.

The experimental MS data are collected in *Table 4*. The mono-Tpy-conjugated strand **5** was analyzed first by MALDI-Q-TOF-MS. Before metallation, a mono-isotopic peak at *m*/*z* 3361.75 was observed ($[M-H]^-$; calc. 3361.75). After metallation with Fe^{2+} at a metal/oligomer ratio of 1:1, the formation of a 2:1 complex between **5** and Fe^{2+} was indicated by the minor peak at *m*/*z* 6778.27 ($[2\,M+Fe-3\,H]^-$; calc. 6778.34) and the major peak at 3388.60 ($[2\,M+Fe-4\,H]^{2-}$; calc. 3388.67). Similar results were observed for **5m** (the corresponding 2′-*O*-methylated derivative of **5**), with peaks at *m*/*z* 7318.55 and 3658.79, corresponding to the $[2\,M+Fe-3\,H]^-$ (calc. 7318.61) and the $[2\,M+Fe-4\,H]^{2-}$ species, respectively.

We next studied the $(Tpy)_2$ conjugates **7** and **7m**. As expected, the non-metallated species gave rise to mono-isotopic peaks at *m*/*z* 3944.95 ($[M-H]^-$; calc. 3944.98) and 4215.09 ($[M-H]^-$; calc. 4215.07), respectively. Metal complexation was then per-

Table 4. *MALDI-Q-TOF-MS Data of Investigated Oligonucleotide Strands and Duplexes.* For details, see the *Exper. Part.* Uncertainty in *m*/*z*: ±0.01 Da.

Strand	Species	*m*/*z* (obs.)	Mass (calc.)
5	$[M-H]^-$	3361.75	3361.75
5+Fe	$[2\,M+Fe-3\,H]^-$	6778.27	6778.34
	$[2\,M+Fe-4\,H]^{2-}$	3388.60	3388.67
5m+Fe	$[2\,M+Fe-3\,H]^-$	7318.55	7318.61
	$[2\,M+Fe-4\,H]^{2-}$	3658.79	3658.80
7	$[M-H]^-$	3944.95	3944.98
7+Fe	$[M+Fe-3\,H]^-$	3998.91	3998.89
7m	$[M-H]^-$	4215.09	4215.07
7m+Fe	$[M+Fe-3\,H]^-$	4268.99	4268.98
2+**7**+Zn	$[\mathbf{2}-H]^-$	2653.45	2653.46
	$[\mathbf{7}+Zn-3\,H]^-$	4006.87	4006.89
	$[\mathbf{7}+2\,Zn-5\,H]^-$	4068.79	4068.81
	$[\mathbf{IIId}+Zn-3\,H]^-$	6666.00	6666.14
	$[\mathbf{IIId}+2\,Zn-5\,H]^-$	6729.00	6728.06
2+**7**+Ni	$[\mathbf{2}-H]^-$	2653.46	2653.46
	$[\mathbf{7}+Ni-3\,H]^-$	4000.87	4000.89
	$[\mathbf{7}+2\,Ni-5\,H]^-$	4056.81	4056.81
	$[\mathbf{IIId}+Ni-3\,H]^-$	6659.00	6659.44
	$[\mathbf{IIId}+2\,Ni-5\,H]^-$	6716.00	6716.11

formed by incubation of single-stranded species with Fe^{2+} at metal/strand ratios of 1:1 or 2:1. Identical results were obtained under both stoichiometric conditions. The corresponding mass spectrum of **7** is shown in *Fig. 4*. The mono-isotopic peaks for strands **7** and **7m** were observed at *m/z* 3998.91 ($[M+Fe-3\,H]^-$; calc. 3998.89) and 4268.99 ($[M+Fe-3\,H]^-$; 4268.98), respectively. Hence, only 1:1 complexes between $(Tpy)_2$-conjugated strands and Fe^{2+} were observed. To exclude the presence of larger oligomers, the same experiment was also studied by means of MALDI-TOF-MS, which allows one to detect *m/z* signals of up to 10,000. Thus, Fe^{2+} or Zn^{2+} were added to strand **7** at a metal/strand ratio of 2:1. In each case, however, only the corresponding 1:1 complexes were observed, with *m/z* values of 4001.9 for $[M+Fe-3\,H]^-$ and 4010.8 for $[M+Zn-3\,H]^-$, with calculated values of 4000.8 and 4010.4 Da, respectively. No signals of higher mass were ever observed. However, after incubation of Zn^{2+} at a Zn/strand ratio of 2:1, a small peak at *m/z* 4073.4 corresponding to a bis-metallated species ($[M+2\,Zn-5\,H]^-$; calc. 4073.8), was detected.

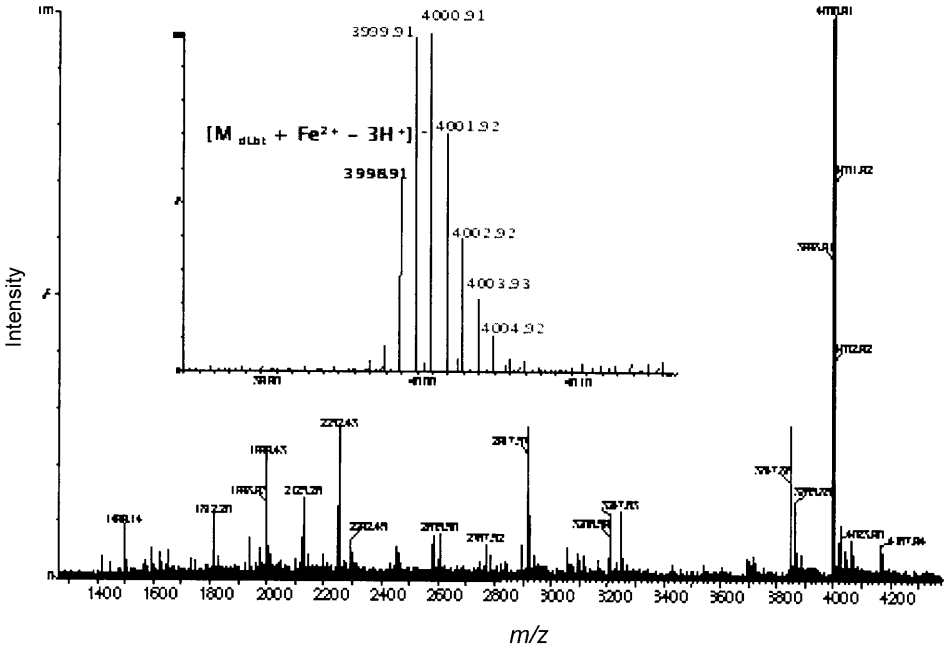

Fig. 4. *MALDI-Q-TOF Mass spectrum of strand* **7** *after metallation with* Fe^{2+}. Inset: Isotopic distribution of the main species $[\mathbf{7}+Fe-3\,H]^-$ (see *Table 4*).

We next investigated double-stranded complexes (see *Table 4*), especially Zn^{II}-metallated species. For MALDI-Q-TOF MS analysis, complex **IId** was annealed at a 1:1 metal/duplex ratio, under the same conditions as those used for the T_m measurements (see above). The observed main peak at *m/z* 2653.45 corresponds to the target strand **2** ($[M-H]^-$; calc. 2653.46). Two minor peaks were detected at *m/z* 4006.87 and 4068.79, corresponding to the $(Tpy)_2$-type oligomers ($[M+Zn-3\,H]^-$ and $[M+2\,Zn-5\,H]^-$).

The full complex **IId** was detected as a minor peak at *m*/z 6666.00 ([**IIId** + Zn − 3 H]$^-$; calc. 6666.08). The same experiment was then repeated with **IId**, but annealed in the presence of an excess of Ni^{2+} at a metal/duplex ratio of 2 : 1. As above, the main isotopic peak at *m*/*z* 2653.46 corresponded to strand **2**. We noticed a clear increase in the intensity of the isotopic peaks at *m*/*z* 4000.87 ([**7** + Ni − 3 H]$^-$; calc. 4000.89) and 4056.81 ([**7** + 2 Ni − 5 H]$^{2-}$; calc. 4056.81). Additional, but very weak, signals were detected at *m*/*z* 6659 and 6716 due to complexes of type [**IIId** + Ni − 3 H]$^-$ and [**IIId** + 2 Ni − 5 H]$^-$ (calc. 6659.44 and 6716.11, resp.; see *Table 4*). Non-metallated species could not be detected.

2.5. *Gel-Shift Analysis.* Gel-shift analysis by polyacrylamide-gel electrophoresis (PAGE) was used to characterize the molecular species involved in the type-II duplexes. *Fig. 5*, *a* shows the PAGE analysis of single strands (**1r**, **3m**, **5m**, **7m**) incubated under either metal-free conditions (EDTA-completed buffer) or in the presence of Fe^{2+} before gel loading. Lanes *1*–*3* and *6* in *Fig. 5*, *a* correspond to the non-metallated species, lanes *1* and *6* being the target RNA strand (13 nucleotides) and the unconjugated 2′-*O*-methylated complementary strand (9 nucleotides), respectively. Lanes *2* and *3* correspond to the mono- and bis-Tpy-conjugated strands. They are separated according to their molecular weight. Finally, lanes *4* and *5* show the band shifts observed upon incubation of 1 equiv. of Fe^{2+} with each **7m** and **5m**, respectively.

The slowest-moving band (*Fig. 5*, *a*, lane *5*) corresponds to the mono-Tpy conjugate, as expected for an intermolecular complex '[Fe^{II}(**5**)$_2$]' of double chain length. In contrast, a fast-moving band (lane *4*) was observed for the bis-Tpy conjugate **7m**, when

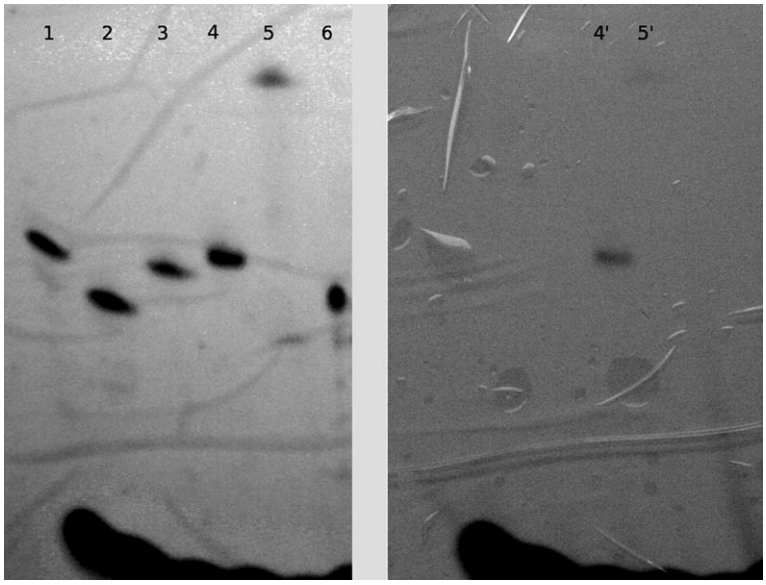

Fig. 5. *Gel electrophoresis of different duplexes under denaturing conditions* (20% polyacrylamide, *Tris* buffer (pH 8.4)). Visualization by *a*) UV shadowing or *b*) under daylight. Lanes *1*,*1′*: **1r**, lanes *2*, *2′*: **5m**, lanes *3*,*3′*: **7m**, lanes *4*,*4′*: **7m** + Fe^{2+}, lanes *5*,*5′*: **5m** + Fe^{2+}; lanes *6*,*6′*: **2m**. The purple-colored spots in lanes *4′* and *5′* are typical for Fe^{II}-Tpy complexes.

metallated with Fe^{2+}, with a mobility close to that of non-metallated **7m**. Fe^{II}–Tpy complexes were easily detected on the same gels thanks to their highly colored (purple) octahedral complexes (*Fig. 5,b*). The lanes *1′–6′* refer to the same samples as lanes *1–6* in *Fig. 5,a*, but visualized under daylight. A faint spot was observed for lane *5′*, apparently due to diffusion, as observed for lane *5*. Both the monomeric nature and the metallation of the molecular species of the spot (lane *4*) were confirmed by elution and MALDI-Q-TOF-MS analyses (*m/z* 4268.99). Elution of the band on lane *5* confirmed the high molecular weight of '$[Fe^{II}(\mathbf{5})_2]$' (*m/z* 7318.55 and 3658.79). Similar results were obtained with DNA strands **1**, **5**, and **7** (data not shown).

2.6. *NMR Experiments.* We report here some preliminary NMR analyses of selected duplexes. Specifically, we chose **0a**, **Ia**, and **IIa** to carefully determine the impact of Tpy conjugates on theses double-stranded structures. The non-metallated duplexes **Ia** and **IIa** were compared to the metallated one. Samples were prepared on a 0.8-mM scale, and 1D- and 2D-NMR spectra were acquired in buffered H_2O/D_2O 9:1 (10 mM phosphate buffer, pH 7.0) at 277 K. When needed, Zn^{2+} was added stepwise until a metal/Tpy stoichiometry of 1:2 was reached.

In a first analysis, the imino H-atoms were monitored, which were assigned primarily from the corresponding imino–imino 2D-NOESY cross-peaks. *Fig. 6* shows the exchangeable imino region at δ(H) 11 – 15 in the ^{1}H-NMR spectrum for the three studied duplexes, either under metal-free conditions or after Zn^{2+} complexation.

2.6.1. *Duplex* **0a**. Base pairs were numbered according to *Fig. 6*, and the imino H-atoms were then numbered according to the base-pair numbers. For example, the imino H-atoms H–N(1) of G^2 and H–N(3) of T^4 are simply referred to as G^2 and T^4, respectively. All expected base pairs were detected on the duplex, as deduced from the peaks found in *Fig. 6,a*. Imino–imino NOE cross-signals occurred sequentially, allowing the assignment of all imino resonances. The imino H-atom of the G^2 base pair, which resonates at δ(H) 12.09, served as a starting point for the assignment (*Fig. 7*). A clear overlap was observed for T^3 and T^8. As a result of exchange with the solvent, cross-peaks for G^1 and G^9 were absent in the 2D-NOESY spectrum, and their imino resonances exhibited a significant broadening compared to the other imino signals, but could, nevertheless, be clearly detected. The corresponding chemical shifts are collected in *Table 5*. Note that G^1 and G^9 assignments are reversible.

2.6.2. *Duplex* **Ia**. In duplex **Ia**, which includes a 3′-Tpy ligand on the shorter strand **5** (*Table 1*), the guanine (G) resonances were clearly affected and significantly broadened (*Fig. 6,b*). The G^1, G^9, and G^2 lines could not be assigned, exhibiting significant broader line-widths. In contrast, the central G^6 resonance was not perturbed. The thymine (T) imino region of the spectrum was also affected. The imino resonances of base pairs *3* and *4*, localized in the vicinity of the Tpy conjugate, were broadened, in contrast to those located at the opposite duplex end (T^7 and T^8), with the T^5 resonance being only slightly broadened. As is evident from *Table 5*, some resonances were shifted in comparison to those of the duplex **0a**, the chemical-shift variations correlating with those in line-width. The observed upfield shifts of the imino resonances decreased from G^2 to T^5, with $\Delta\delta$ values of 0.26 to 0.05 ppm.

2.6.3. *Duplex* **IIa**. The 1D-NMR spectrum of **IIa** showed only five resonances (*Fig. 6,c*). They were assigned to the 5′-end of the $(Tpy)_2$-conjugated oligomer (strand **7**; *Table 1*). Surprisingly, the terminal G^9 base pair was easily detected, exhibiting a

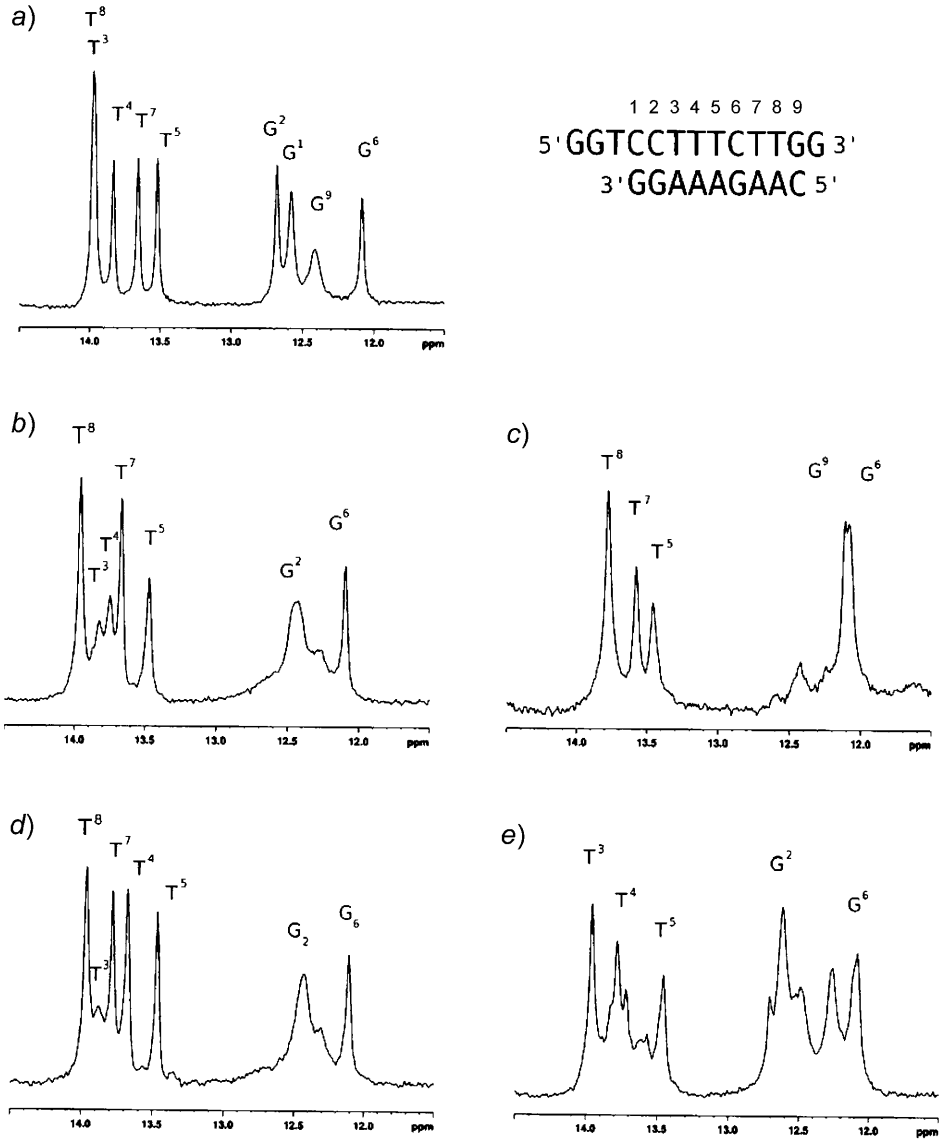

Fig. 6. *^{1}H-NMR Resonances of the exchangeable imino region* (δ(H) 11–15 ppm) *of duplexes* a) **0a**, b) **Ia**, c) **IIa**, d) **Ia**/Zn^{2+} (1 equiv.), *and* e) **IIa**/Zn^{2+} (1 equiv.). The base-pair numbers shown also apply to the imino H-atoms (see text).

sharp resonance. The G^6 resonance line was not perturbed, and exhibited similar characteristics for the three duplexes (**0a**, **Ia**, **IIa**), both in terms of line-width and chemical shift (*Table 5*). Among the five expected lines of the thymine base pairs, only three were detected (T^5, T^7, and T^8), the signals for T^5 and T^7 being slightly broadened compared to those for **Ia** (*Fig. 6*, *b*). Comparison between duplexes **0a** and **IIa** further revealed an

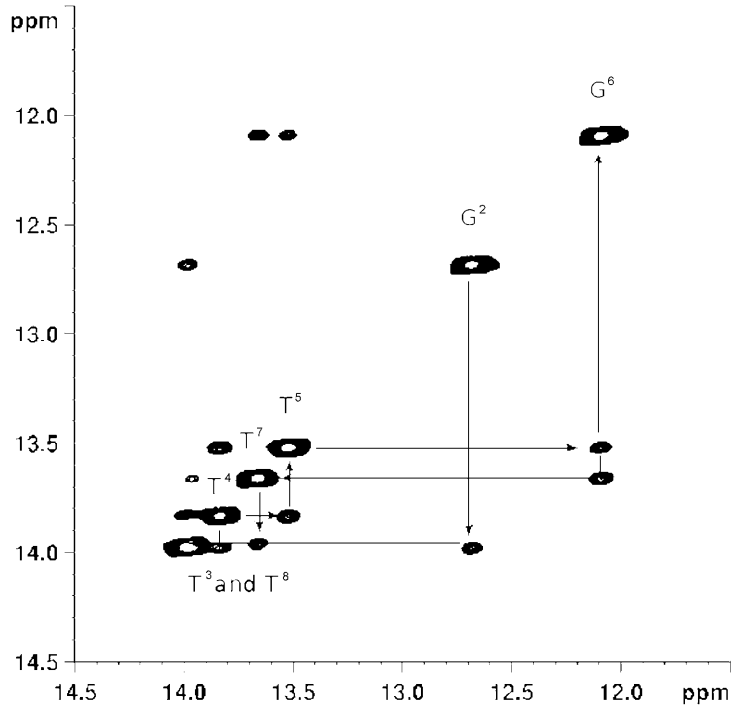

Fig. 7. *2D-NOESY Map of the expanded imino–imino region of the duplex* **0a**. Solvent: H_2O/D_2O 9:1. The lines indicated NOEs along spatially neighbored imino H-atoms (numbered according to the base pairs).

Table 5. *^{1}H-NMR Chemical Shifts* (δ(H) [ppm]) *of the Imino Resonances in Various Duplexes.* For strand numbering and sequence, see *Fig. 6* and *Table 1*. Asterisks (*) denote assignments that may be interchanged. ΔT_m values ($= T_m$ (**0a**) $- T_m$ (**Ia** or **IIa**)) are given in parentheses.

Duplex	G^1	G^2	T^3	T^4	T^5	G^6	T^7	T^8	G^9
0a	12.58*	12.68	13.97	13.83	13.52	12.09	13.66	13.97	12.41*
Ia		12.42	13.82	13.75	13.47	12.09	13.66	13.96	
		(0.26)	(0.15)	(0.08)	(0.05)				
IIa					13.45	12.09	13.57	13.77	12.11
					(0.07)	(0)	(0.1)	(0.2)	(0.3)
Ia + Zn		12.43	13.88	13.75	13.47	12.10	13.67	13.96	
IIa + Zn		12.61	13.94	13.77	13.45	12.08			

upfield shift of the resonances close to the 5′-Tpy ligand, with $\Delta\delta$ values ranging from 0.3 to 0.07 ppm. The shift regularly decreased from the 5′-end to the core of the duplex.

Next, we studied the metallated duplexes **Ia** and **IIa** upon addition of 0.5 equiv. of Zn^{2+} relative to the Tpy ligands. The corresponding 1D-NMR spectra are shown in *Fig. 6,d* and *6,e*, respectively. We first studied the impact of metallation on the mono-Tpy-conjugated duplex **Ia**. Under the experimental conditions used, an intermolecular metal complex between two duplexes was expected. The observed imino-resonance

pattern closely resembled that observed for the non-metallated species (compare *Fig. 6,b* with *Fig. 4,d*). The main NMR features of metallated **Ia** were sharper resonances for T^3, T^4, and T^5, as well as minor variations in chemical shift (*Table 5*), compared to the non-metallated duplex.

The NMR imino regions of metallated and non-metallated **IIa** are shown in *Fig. 6,e* and *Fig. 6,c*, respectively. The spectrum of the metallated form was found to have more resonance lines both for the G and T regions. This might be due to an equilibrium between two or more structures in the NMR sample. We could assign five main resonances supposed to belong to the major component of the putative mixture. These resonances (G^2, T^3, T^4, T^5, and G^6) were located at the 3′-end of the $(Tpy)_2$-conjugated strands, the observed chemical shifts being close to those found for the unmodified duplex **0a**. The metallation of duplex **IIa** was checked by MALDI-TOF-MS analysis (negative mode), which gave a major peak at m/z 4010.4 ($[M+Zn-3\,H]^-$; calc. 4010.40), in full accordance with a mono-metallated $(Tpy)_2$ conjugate.

3. Discussion. – We have previously demonstrated that high-affinity metal chelators containing one or two terpyridine (Tpy) residues [17] can be used to assemble and stabilize two complementary oligonucleotides [12][14]. The conjugation of Tpy moieties to stem-loop oligomers provides an efficient procedure for metal-templated cyclization of oligomers. Herein, we report an extension of this concept by studying the potential of 3′,5′-(Tpy) conjugated oligonucleotides to wrap around a complementary strand, when linked through metal coordination.

In order to allow such a cyclization, we conceived specific linkers between the Tpy moiety and the terminal OH groups of the oligonucleotides. These linkers were optimized through molecular modeling. As shown in *Fig. 1,b*, a one-turn helical duplex places the Tpy ligands in a face-to-face position, which, when coordinated to a metal ion, leads to a circularized oligonucleotide, the complementary strand passing through this circle. This topology is a prerequisite for the formation of a catenane, when the target strand is also a circular oligonucleotide. In a recent paper by *Göritz* and *Kramer* [18], a complementary approach was developed: a $(Tpy)_2$-conjugated DNA strand was circularized through metal chelation such that, due to conformational restrictions, double-helix formation was prevented. The complementary sequences used involved the formation of a 15-bp duplex, which corresponds to a 1.5 double-helical turn, placing the Tpy moieties at opposite positions along the duplex. The short and non-optimized arms these authors used for the links between the 3′- and 5′-terminus of the $(Tpy)_2$-conjugated strands will not favor the chelation of the Tpy units, when hybridized to the complementary sequence.

In this work, we designed a simplified system to rationalize the conformational restrictions of such a topological object. We chose to explore the two main helical forms of nucleic acid helices by studying both *B*-DNA duplexes and the *A*-RNA conformation of an RNA 2′-*O*-methyl hybrid [19]. The 9-bp model chosen was derived from an apical loop from the HCV genome. It fulfils the above criteria, *i.e.*, a length close to a one-turn double-helical duplex. We then analyzed the molecular species involved in the metallated duplexes through various techniques.

MS Analyses allowed us to show that the species resulting from metal addition to the bis-Tpy-conjugated single strands **7** and **7m** were 1:1 complexes between metal

and oligomer (*Table 4*). This well-defined stoichiometry could account for either a monomeric (1+1) intramolecular metallo-macrocycle or oligomeric ($n+n$) species. As we could not detect higher-molecular-weight entities by MS analysis, we tried to confirm the molecular size of the metallic complex by gel-shift analysis under denaturation conditions. The mobility of the band for **7m** in the presence of Fe^{2+} (*Fig. 5*, *a*, lane *4*) is in full concordance with a monomeric compound, metallation being easily detected both by coloration as well as MS analysis after elution of the spot. Taken together, these data led us to conclude that **7** and **7m** strands are fully circularized under the experimental conditions used. Although our experimental data do not discard the simultaneous occurrence of a mono-Tpy complex and a non-metallated one, the thermodynamic data do not support this possibility, particularly for Fe^{II} complexes [17].

Thermal-melting experiments allowed us to analyze the response of the circularized oligomer when annealed to its complementary strand. Data obtained from DNA duplexes (*Table 2*) underline a specific behavior of the $(Tpy)_2$-conjugated oligomers, when incubated with their target strand in the presence of metal ions. At low temperature, circularized Tpy-oligomers are paired to their targets. The observed destabilization of these duplexes (**IIa**) in comparison with unmodified duplexes (**0a**) or a mono-conjugated oligomer (**Ia**) is correlated with the occurrence of the coordination link between the two terminal Tpy moieties. The release of this constraint by disruption of the link between the two Tpys (by addition of a slight excess of Ni^{2+}) is associated with a raise in melting temperature (T_m), reaching those observed for unconjugated or metal-free duplexes. We, thus, conclude that the circularized metallated oligomer is annealed to its complementary strand.

Furthermore, the 2′-*O*-methylated, circularized oligomer was able to anneal to its targeted RNA strand, reaching a T_m value close to that of the unmodified duplexes (*Table 3*). This was observed first by adding Mg^{2+} to the incubation medium. The Mg dependence of RNA folding and RNA-strand association is well documented [20][21]. However, we never observed such a dependence for DNA duplexes (**IIa**–**c**; data not shown). When we tried to release the putative conformational constraint by inclusion of unpaired nucleotides (T or U) at one or both ends of strands **8m** and **9m**, the corresponding duplexes (**IIrb**, **IIrc**) melted at higher temperatures after metal addition (*Table 3*). Such an effect was not observed for duplexes **IIb** and **IIc**. Additive effects were observed upon Mg^{2+} addition to these extended strands. These effects both suggest that the conception and design of the link between the Tpy moieties and the oligonucleotides deserve further studies.

Duplex formation on the circularized oligomer **7** was clearly corroborated also by NMR experiments. Base pairs were easily detected through the imino H-atom resonances [22]. As shown in *Fig. 6*, the duplex **IIa** showed at least five imino resonances at δ(H) 11–14 at low temperature (0°). This led us to suggest that mixtures of closely related helical conformers are formed after metal addition to **IIa**. This observation precluded further NMR analysis of the structure of the complex between the annealed strands. We are, thus, currently unable to precisely describe the association topology, and it remains uncertain whether or not *Fig. 2* provides a realistic representation of the structure.

The NMR experiments revealed some further interesting observations. According to melting-temperature experiments, 3′- and/or 5′-conjugation of Tpy units results, at least in the absence of metal ions, in a slight increase in T_m of the corresponding duplexes (*Table 2*). 5′-Conjugation is generally more efficient in this stabilization, as reported before [14]. The NMR data showed an increase in the dynamics of base pairs located close to the 3′-conjugation site, and an increase in life time of the base pairs located at the 5′-terminus. On both ends of duplex **IIa**, an upfield shift of the imino resonances was observed, relative to those of **0a**. These observations suggest a different mode of interaction of Tpy with the double strand when located at the 3′- *vs.* the 5′-end, correlating with differences in the stabilization abilities of these conjugates. Although the upfield NMR shifts of the imino resonances upon conjugation of Tpy suggest an intercalative binding mode [23], we never noticed clear stabilizing properties of free Tpy ligands for double-stranded DNA [12]. A *partial* dynamic intercalation of non-metallated Tpy could account for the observed dynamics of the base pairs at the 3′-end. Stacking of the 5′-Tpy residue on the last base pair could contribute to the sharper resonance observed for the imino H-atoms of G^9 on the duplex **IIa**. However, an interaction of both Tpys within the minor or major groves cannot be fully excluded [24]. Only a complete structural analysis of such a duplex will allow a more comprehensive understanding of these experimental data.

4. Conclusions. – We have shown that a short, synthetic, single-stranded oligonucleotide bearing terminal terpyridine moieties is easily cyclized through metallation and can be used to target DNA or RNA strands. Our study underlines that the link between the Tpy moieties and the 3′- and 5′-ends of the oligomers must carefully be designed to allow a thermodynamically favorable association between the single strands after metallation. More studies have to be conducted to design new links taking into account both the nature of the targeted strand and the chemistry of the synthetic circular strand. In this last objective, the use of 2′-*O*-methylated RNA seems to be the most promising approach to design efficient circular ligands for RNA.

Experimental Part

Oligonucleotide Synthesis. The unmodified oligonucleotides were purchased from *Eurogentec*. All modified oligonucleotides were synthesized on a 0.2-μmol scale on a *Millipore Expedite-8909* DNA synthesizer using conventional β-cyanoethyl phosphoramidite chemistry. The modified and standard bases were dissolved in anh. MeCN (0.1M final concentration). The modified phosporamidites were coupled manually, with a coupling time of 15 min. The coupling efficiency was the same as that for the unmodified amidites. All oligomers were synthesized in the 'trityl-off' mode. Standard deprotection procedures were used according to DNA and RNA sequences. The crude oligonucleotides were purified by electrophoresis on denaturing (20%) polyacrylamide gel, and the pure samples were desalted with the aid of reverse-phase *Maxi-Clean* C_{18} cartridges (*Altech*).

Melting Experiments. The purified oligonucleotides (each strand 1 μM) were diluted in 0.5 ml buffer (10 mM phosphate buffer (pH 7), 150 mM NaCl, 100 μM EDTA (metal-free experiments)); all other experiments were performed with the same buffer, but in the absence of EDTA. Metal addition was carried out by adding aliquots of a metal-salt soln. The mixtures were heated at reflux for 2 min, and hybridization was assured by cooling the sample to low temperature. Melting experiments were performed with a *Cary-1E* UV/VIS spectrophotometer equipped with a temp. controller. Samples were pre-equilibrated

at 4° for at least 30 min, and then heated from 4 to 90° at a rate of 0.4°/min. The absorbance at 260 nm was recorded every 30 s. The melting temperature was determined by means of graphical methods [4], and the reported data are the mean from at least three experiments.

Mass Spectrometry. MALDI-Q-TOF Mass spectra were performed on a *Waters Ultima* spectrometer, with negative-ion detection, using reference oligonucleotides for mass calibration and an accuracy better than ±0.01 Da. A special preparation technique was designed to analyze the Tpy-modified oligonucleotides. The stainless-steel target was first covered with a thin layer of matrix (0.5 µl of 2,4,6-trihydroxyacetophenone (THAP) at a concentration of 10 mg/ml in acetone), and this layer was washed with standard EDTA soln. (2×1 µl) and H_2O (2×1 µl). The oligonucleotides (0.8 µl of a 20 µM soln. in H_2O) were then deposited on this matrix layer and allowed to dry. The final preparation step was the application of a second layer of matrix (0.8 ml of a 4:1 soln. of THAP (10 mg/ml in EtOH) containing 100 mM aq. ammonium citrate), followed by drying at r.t. MALDI-TOF measurements were performed with a *Bruker Reflex-III* instrument. The same sample preparation as described above was used for all Tpy-conjugated oligonucleotides.

Gel-Shift Assay. Gel-shift analyses were performed in denaturing 20% polyacrylamide gel using *Tris* buffer (pH 8.4). The electrophoresis was carried out at 200 or 150 V and at a temp. of 4°. The gel bands were visualized under UV light, or under daylight in the case of colored Tpy–Fe complexes.

NMR Spectroscopy. NMR Experiments were performed on a 500-MHz *Bruker Avance* spectrometer with a *z*-gradient *TXI* probe. Samples were prepared on a 0.8-mM scale, and 1D- and 2D-NMR spectra were acquired in H_2O/D_2O 9:1. The pH of all solns. was adjusted to 7.0 with 10 mM sodium phosphate buffer. When needed, Zn^{2+} was added stepwise, until a metal/Tpy stoichiometry of 1:2 was reached. All spectra were recorded at 273 K. 2D-NMR spectra of the imino region were recorded after a mixing time of 300 ms. A combination of Watergate and Jump-and-Return sequences was used for water suppression [25]. The chemical shifts were calibrated against 3-(trimethylsilyl)(D_4)propanoic acid (TSP). All spectra were collected in phase-sensitive mode using the STATES-TPPI method, and processed with the TOPSPIN software.

Structure Calculation. Energy minimizations were used to optimize the Tpy-modified oligomer ligand to be wrapped around the targeted strand. The calculations were performed on a *Silicon Graphics Fuel* workstation using the DISCOVER module of INSIGHTII (*Accelrys*), applying the CVFF forcefield. The initial complex was build starting from an ideal *A*-type double-helical model. The Tpy–metal coordination was constrained according to literature data [16].

REFERENCES

[1] R. T. Batey, R. P. Rambo, J. A. Doudna, *Angew. Chem., Int. Ed.* **1999**, *38*, 2327.
[2] J. J. Toulmé, C. Di Primo, S. Moreau, *Prog. Nucl. Acid Res. Mol. Biol.* **2001**, *69*, 1.
[3] P. Svoboda, A. D. Cara, *Cell Mol. Life Sci.* **2006**, *63*, 901.
[4] J. L. Mergny, L. Lacroix, *Oligonucleotides* **2003**, *13*, 515.
[5] C. Dietrich-Buchecker, J. Sauvage, *Chem. Rev.* **1987**, *87*, 795.
[6] F. Vögtle, T. Dünnwald, T. Schmidt, *Acc. Chem. Res* **1996**, *29*, 451.
[7] G. R. Newkome, T. J. Cho, C. N. Moorefield, P. P. Mohapatra, L. A. Godinez, *Chem. – Eur. J.* **2004**, *10*, 1493.
[8] H. Hofmeier, R. Hoogenboom, M. E. Wouters, U. S. Schubert, *J. Am. Chem. Soc.* **2005**, *127*, 2913.
[9] J. Sauvage, J. Collin, J. Chambron, S. Gillerez, C. Coudret, *Chem. Rev.* **1994**, *94*, 993.
[10] J. M. Berg, Y. Shi, *Science* **1996**, *271*, 1081.
[11] R. Hogg, R. Wilkins, *J. Chem. Soc.* **1962**, 341.
[12] L. Zapata, K. Bathany, J. M. Schmitter, S. Moreau, *Eur. J. Org. Chem.* **2003**, *6*, 1022.
[13] A. V. Pisarev, N. E. Shirokikh, C. U. Hellen, *C. R. Biol.* **2005**, *328*, 589.
[14] F. Freville, N. Pierre, S. Moreau, *Can. J. Chem.* **2006**, *84*, 854.
[15] N. N. Dioubankova, A. D. Malakhov, D. A. Stetsenko, V. A. Korshun, M. J. Gait, *Org. Lett.* **2002**, *4*, 4607.
[16] A. T. Baker, H. A. Goodwin, *Aust. J. Chem.* **1985**, *38*, 207.
[17] R. Holyer, C. Hubbard, S. Kettle, R. Wilkins, *Inorg. Chem.* **1966**, *5*, 622.

[18] M. Goritz, R. Kramer, *J. Am. Chem. Soc.* **2005**, *127*, 18016.
[19] M. Egli, *Angew. Chem., Int. Ed.* **1996**, *35*, 1894.
[20] D. Lilley, *Biopolymers* **1998**, *48*, 101.
[21] P. B. Moore, *Annu. Rev. Biochem.* **1999**, *68*, 287.
[22] D. Wemmer, in 'Nucleic Acids: Structures, Properties, and Functions', Eds. V. Bloomfield, D. Crothers, I. Tinoco, University Science Books, Sausalito, CA, 1999, p. 111.
[23] J. Feigon, W. A. Denny, W. Leupin, D. R. Kearns, *J. Med. Chem.* **1984**, *27*, 450.
[24] W. D. Wilson, F. A. Tanious, R. A. Watson, H. J. Barton, A. Strekowska, D. B. Harden, L. Strekowski, *Biochemistry* **1989**, *28*, 1984.
[25] D. Collin, C. Heijenoort, C. Boiziau, J. Toulme, E. Guittet, *Nucleic Acids Res.* **2000**, *28*, 3386.

Received August 28, 2006